Highly Stereospecific On-Surface Dimerization into Bishelicenes: Topochemical Ullmann Coupling of Bromohelicene on Au(111)

Voigt, Jan ; Martin, Kévin ; Neziri, Egzona ; Baljozović, Miloš ; Wäckerlin, Christian ; Avarvari, Narcis ; Ernst, Karl-Heinz

DOI: https://doi.org/10.1002/chem.202300134

Chemistry–A European Journal
Research Article
doi.org/10.1002/chem.202300134
Chemistry Europe
European Chemical Societies Publishing
www.chemeurj.org

Highly Stereospecific On-Surface Dimerization into Bishelicenes: Topochemical Ullmann Coupling of Bromohelicene on Au(111)

Jan Voigt,[a] Kévin Martin,[b] Egzona Neziri,[a] Miloš Baljozović,[a] Christian Wäckerlin,[a] Narcis Avarvari,*[b] and Karl-Heinz Ernst*[a, c, d]

In memoriam Ursula Ellerbeck

Abstract: The on-surface dimerization into bis(hexahelicene) on a gold(111) surface has been studied by means of scanning tunneling microscopy and time-of-flight secondary mass spectrometry. C–C Ullmann coupling of (*rac*)-2-bromo-hexahelicene leads to formation of the *(M,M)*- and *(P,P)*-diastereomers of 2,2′-bis(hexahelicene), whilst formation of the *(M,P)*-diastereomer is not observed. Upon cooling, the bis(hexahelicene) aggregates into an ordered two-dimensional lattice with partly randomly distributed enantiomers. The highly specific diastereomeric coupling is explained by the surface alignment of educt in combination with the strong steric overcrowding in a possible surface-confined *(M,P)*-product.

Introduction

Solid-state chemistry in confined environments, such as crystals or interfaces between crystallites, are the classical examples of topochemistry.[1] However, topochemical constraint may be also introduced by relative alignment of molecules on a surface or by their dense lateral packing, thus causing stereoselectivity.[2]

On-surface chemistry has become a popular synthesis strategy to achieve new functional materials and interfaces that are hardly available by solution chemistry.[3] Prominent examples are graphene nanoribbons, nanographenes and macrocycles.[4] Such systems are usually obtained by *in-vacuo* deposition of aromatic precursors onto metal surfaces followed by thermally induced C–C coupling. In that respect, the Ullmann coupling has been extremely powerful and became the main route towards two-dimensional polymeric carbon structures.[5] Adatoms of gold, silver or copper surfaces activate thereby a C–X bond (X=Br, I) and establish an organometallic intermediate between the adatom and two dehalogenated educts before final C–C coupling.

Helicenes represent a very important class of aromatic compounds endowed with molecular helical chirality resulting from the *ortho*-condensation of aromatic rings along a helical axis.[6] Their interest is mainly related to their exceptional chiroptical properties and rigid helical structure,[7] making them precursors of prime importance for self-assembly and chiral recognition on surfaces,[8] chiral photonics,[9] circularly polarized emission[10,11] or chirality induced spin selectivity (CISS).[12,13] The straightforward access to bis- or tris-helicenes with specific configurations is therefore particularly interesting, but generally challenging when starting from racemic mixtures of precursors, yet the on-surface chemistry offers such synthetic control in the Ullmann coupling of bromo-helicenes.[14,15]

In a previous on-surface Ullmann coupling study with 9-bromo-heptahelicene a slight selectivity towards the *(M,P)*-diastereomer has been reported.[16] Here it is shown by means of scanning tunneling microscopy (STM) that Ullmann coupling of (*rac*)-2-bromo-hexahelicene (Br[6]H, Figure 1a) on a gold(111) surface leads exclusively to the homochiral combinations of *(M,M)*- and *(P,P)*-bis(hexahelicene) (bis[6]H, Figure 1b). C–C coupling into the *(M,P)*-diastereomer is not observed (Figure 1c). Forcefield based molecular dynamics simulations support these findings by showing that surface-alignment installs a large energy penalty due to strong steric constraint in the *(M,P)*-diastereomer. The present study here therefore highlights the

[a] Dr. J. Voigt, E. Neziri, Dr. M. Baljozović, Dr. C. Wäckerlin, Prof. Dr. K.-H. Ernst
Molecular Surface Science and Coating Technology Laboratory
Empa, Swiss Federal Laboratories for Materials Science and Technology
Überlandstrasse 129, 8600 Dübendorf (Switzerland)
E-mail: karl-heinz.ernst@empa.ch

[b] Dr. K. Martin, Prof. Dr. N. Avarvari
MOLTECH-Anjou
UMR 6200, CNRS, UNIV Angers
2 bd Lavoisier, 49045 Angers Cedex (France)
E-mail: narcis.avarvari@univ-angers.fr

[c] Prof. Dr. K.-H. Ernst
Nanosurf Laboratory, Institute of Physics
The Czech Academy of Sciences
Cukrovarnická 10, 162 00 Prague (Czech Republic)

[d] Prof. Dr. K.-H. Ernst
Department of Chemistry, University of Zurich
Winterthurerstrasse 190, 8057 Zürich (Switzerland)

Supporting information for this article is available on the WWW under https://doi.org/10.1002/chem.202300134

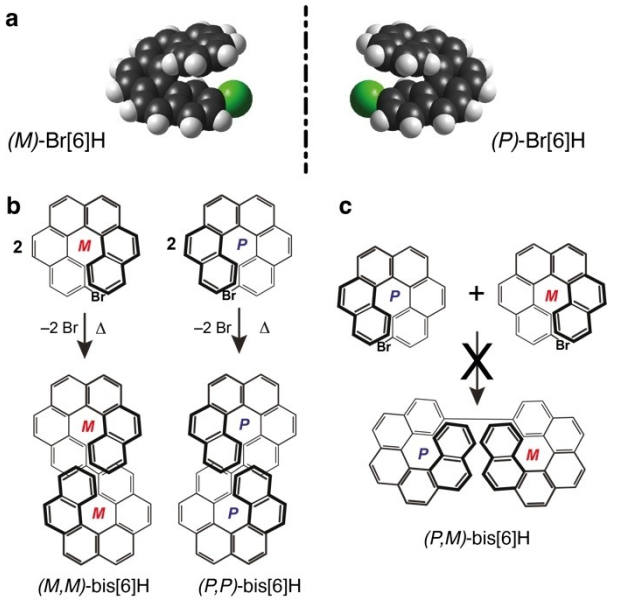

Figure 1. (a) Full-space models of 2-bromo-hexahelicene enantiomers (Br-[6]H). (b) Sketch of the enantiospecific on-surface Ullmann coupling of 2-bromo-hexahelicene into *(M,M)*- and *(P,P)*-2,2′-bis(hexahelicene) enantiomers. (c) The dimerization into the *(M,P)*-diastereomers is not observed.

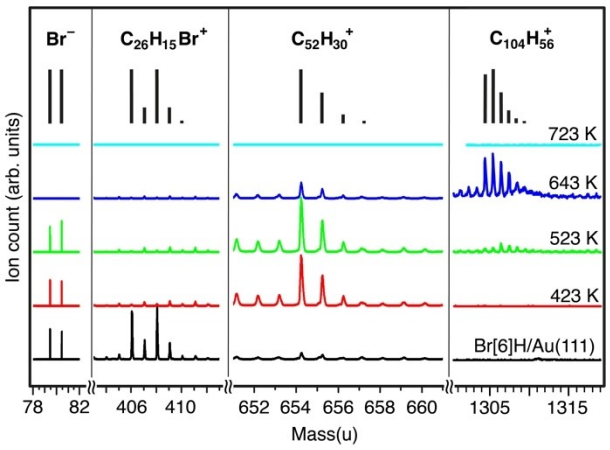

Figure 2. ToF-SIM spectra acquired from Br[6]H on Au(111). Bromine (Br^-), Br[6]H ($C_{26}H_{15}Br^+$) and bis[6]H ($C_{52}H_{30}^+$) mass regions are shown. The expected mass distributions are displayed by black bars. After deposition at room temperature, the sample is stepwise annealed for 5 min to the indicated temperatures. Appearance of mass 654 amu at 423 K shows formation of bis[6]H on the surface. The group at 1305 amu represents a $(bis[6]H)_2$/-4H species indicating further dehydrogenation at higher temperatures.

importance of the position of the bromine at the rim of the helical backbone in order to impose a large stereoselectivity during on-surface C–C coupling.

Results and Discussion

The thermally induced on-surface chemistry of (*rac*)-Br[6]H has been evaluated at first with time-of-flight secondary ion mass spectrometry (ToF-SIMS) and X-ray photoelectron spectroscopy (XPS). Br[6]H was intactly deposited by sublimation and shows ordered self-assembly (Figure S1 in the Supporting Information). The debromination of Br[6]H is confirmed by a shift in Br 3p binding energy in XPS between 300 K and 420 K (Figure S2). ToF-SIMS shows that annealing to 423 K leads to the formation of bis[6]H ($C_{52}H_{30}$) that remains stable up to 543 K (Figure 2). A potential product of bis[6]H/-2H, which could occur due to additional dehydrogenative C–C bond formation between the two upper terminal benzo-groups, is not observed here. Further annealing to 643 K leads to reduction of the bis[6]H signals and to the appearance of mass signals corresponding to $C_{104}H_{56}^+$ (Figure 2), indicating further dehydrogenation. Such species corresponds to $(bis[6]H)_2$/-4H, possibly formed by dimerization of bis(helicenes) with two additional C–C bonds. However, note that ToF-SIMS is highly sensitive and may show strong signals for species that are not abundant on the surface. In addition, signals corresponding to Br have disappeared. This observation is consistent with previous reports showing that Br desorbs as HBr by reaction with released atomic hydrogen.[17,18]

Post reaction cooling leads to two-dimensional (2D) ordered aggregation of the Ullmann-coupled product on the surface (Figure 3). STM images show that molecules assemble in rows along the high symmetry directions of the Au(111) surface. Hence, rotational domains are observed, whereby the domain boundaries coincide with monoatomic steps of the gold substrate (Figure 3a, Figure S2). The higher-resolution images of each domain show the single bis[6]H product in the form of pairs of bright protrusions (Figure 3b, Figure S3). The molecules assemble in rows with alternating azimuthal tilt angles. In addition, there are bis[6] molecules rotated by $\pm 120°$ with respect to the rows (highlighted in green in Figure 3b). Figure 3c shows the assignment of enantiomers in the rows. That is, although the general STM image contrast does not allow a determination of absolute configuration, handedness can be determined by the assumption of identical surface registry, observed intermolecular distance and STM appearance of the single molecules. A detailed analysis is presented in the Supporting Information (Figure S4). The STM contrast was modelled by extended Hückel theory (Figure 3d, Supporting Information). The structure model in Figure 3d proposes crystallization into rows of alternating handedness, which would result in a 2D racemate crystal. The unit cell is classified here in matrix notation as (5 5,–6 6).[19] Note, that the handedness of bis[6]H molecules highlighted in green could not be identified with certainty. Their random appearance actually classifies this system as a solid solution of enantiomers in a racemate lattice.

The possible reason for the absence of *(M,P)*-diastereomers has been evaluated by molecular dynamics calculation based on Amber force-fields (Figure 4). Already for the free *(M,P)*-isomer the steric constrain is higher than for the *(M,M)*- and *(P,P)*-enantiomers. When aligned on the gold surface, the *(M,P)*-isomer lies even higher in energy with respect to the bis(helicene) enantiomers. The main reason is the smaller

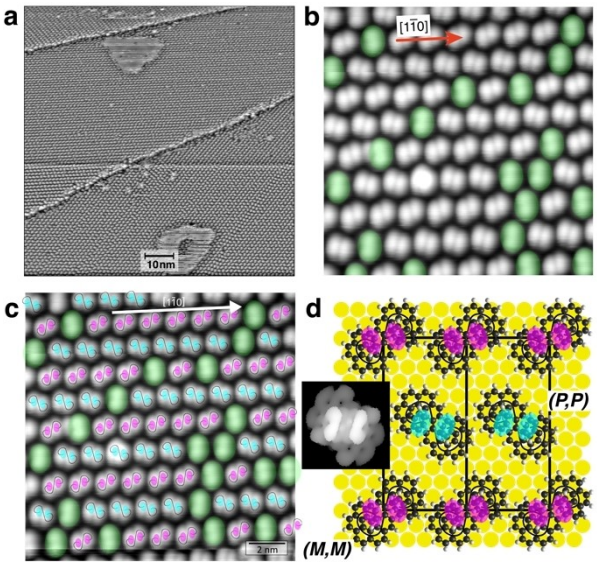

Figure 3. a) STM image of a saturated monolayer of bis[6]H on Au(111) (105 nm × 105 nm, U = 2.83 V, I = 60 pA, T = 120 K). b) STM image (13 nm × 13 nm, U = 2.29 V, I = 50 pA, T = 120 K) from a single domain. Single bis[6]H molecules on the surface are identified as dumbbell-shaped contrast which are arranged in rows with alternating azimuthal tilt angles. Molecules highlighted in green represent a randomly distributed minority with a third azimuthal orientation. c) Assignment of enantiomers to the different rows in a single domain. *(M,M)*-enantiomers and *(P,P)*-enantiomers are marked by two pink and two cyan semitransparent filled ellipses, respectively. The ellipses are placed onto the bright protrusions in the STM image (U = 2.29 V, I = 50 pA, T = 120 K). d) Structure model of alternating enantiopure rows along the [1$\bar{1}$0] direction of the Au(111) surface. Molecules are placed with the Ullmann-coupled C–C bond on top of Au bridge sites. The observed two bright protrusions (mimicked by pink and cyan semitransparent filled ellipses) are assigned to the two distal ends of the bis(helicenes). The inset shows a visualization of a HOMO front orbital of the *(P,P)*-enantiomer as calculated with extended Hückel theory.

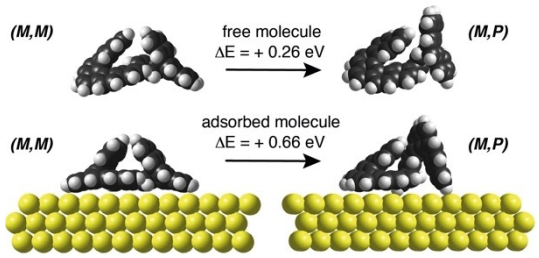

Figure 4. Molecular dynamics simulation of the isolated free space *(M,M)*- and *(M,P)*-diastereomers (top) and in the adsorbed state on a three-atomic-layer slab (bottom). The homochiral combination lies for both cases much lower in energy.

surface contact area which basically determines the extend of the interaction.

Density functional theory and X-ray photoelectron diffraction showed for single penta- and heptahelicene a parallel alignment of the lower phenanthrene group to the surface plane on various Cu, Ag and Au surfaces.[12,20,21] Therefore, the helicenes adopt a configuration in which they spiral away from the surface. Such footprint surface contact has previously been identified for both helical subunits in the case of 2,2′-bis(tetrahelicene), 2,2′-bis(pentahelicene) and 9,9′-bis(heptahelicene) on Cu(100), Au(111) and Cu(111), respectively.[14,16,22,23] Combinations of helicenes of opposite handedness are strongly disfavored because they cannot have contact with their phenanthrene ends parallel to the surface simultaneously during the dimerization reaction. The dehalogenation step of on-surface Ullmann coupling is considered to be a reversible process on Au.[24,25] The resulting extended average radical lifetimes should allow migration of dehalogenated helicenes via other adatoms until they find the suitable counterpart to complete the reaction.

Instead of diastereospecific coupling, an alternative scenario could be unspecific Ullmann coupling followed by conversion into homochiral dimers at the temperature of reaction, i.e., 420 K. In order to explain the absence of *(M,P)*-isomers such conversion into the other diastereomers has been proposed for room temperature deposition of bis[5]H onto Au(111).[23] However, the activation energy for enantiomer inversion for [6]H in solution has been determined to be around 140 kJ/mol.[26] Moreover, with one end bound to the surface this value is expected to be much higher. For the binding energy of a single heptahelicene on Au(111) a value of 140 kJ/mol has been calculated by DFT.[12] (As no van der Waals correction has been applied in that study, the value is expected to be even higher.) A bis(helicene) with both subunits in identical contact with the surface has a binding energy of roughly twice as much, which leads to the conclusion that an interconversion in the adsorbed state for bis[6]H is very unlikely. In order to compare the diastereoselectivity of the on-surface coupling with that in the bulk, in-solution synthesis starting from Br[6]H via a strategy involving a Pd-mediated cross coupling in the presence of boronic ester, as previously performed for 2,2′-bis(pentahelicene),[23] or by a modified Ullmann coupling procedure has been attempted. However, these wet chemistry strategies did not yield the targeted 2,2′-bis(hexahelicene), which remained elusive so far, underlying as well the synthetic interest of using on-surface chemistry to induce C–C coupling.

Conclusion

Adsorption of racemic 2-bromohexahelicene on Au(111) followed by Ullmann coupling into bishexahelicene leads exclusively to the formation of *(M,M)*- and *(P,P)*-enantiomers whereas a *meso-(M,P)* form is not observed on the surface. Molecular dynamics calculation show that the adsorbed *meso*-form would be 0.66 eV higher in energy due to steric overcrowding of the upper parts of the helices. The here reported diastereoselective on-surface reaction is a special example of topochemistry in which the surface alignment of the reactant supports enantiospecific chemistry.

Experimental Section

General procedure: Br[6]H was synthesized in 6 steps from 2-bromomethylnaphthalene according to a described procedure.[27] All experiments were performed on Au(111) single crystals under ultrahigh vacuum conditions. The surface was cleaned by cycles of Ar^+ sputtering and annealing. Samples were prepared by thermal

sublimation of racemic 2-bromohexahelicene onto the clean Au(111) surface from an effusion cell evaporator. Typical evaporation parameters for a monolayer coverage were 413 K for 30 minutes while keeping the sample at 333 K. Scanning tunneling microscopy (STM) experiments were conducted at 120 K with a Specs Aarhus 150 in constant current mode using a tungsten tip. All STM images are calibrated using atomic resolution on Cu(100). Time-of-flight secondary ion mass spectrometry (ToF-SIMS) was performed with an IONTOF ToF-SIMS 5 instrument on in situ prepared samples using a 25 keV beam of Bi_3^+ primary ions. The beam was randomly rasterized over an area of 0.25 mm^2 and an extraction voltage of 3 kV was used. The mass calibration was performed using the Au_n^+ signals of the substrate. The intensity of the spectra was normalized to the Au_3^+ peaks. The pressure during preparation and measurements was below 10^{-8} mbar.

Computational details: The optimized structures of *(P,P)*- and *(M,P)*-dimers of bis[6]H were computed with the molecular mechanics AMBER-type force field of HyperChem 8.0 program. A three-layer Au(111) slab with periodic boundary conditions was used as template, with the gold atoms fixed in space during the calculations. The molecules were enabled to move freely during the optimization. For each dimer, 432 different initial configurations (x, y, z coordinates and azimuthal angle, z = axis normal to the gold surface) were tested. For the geometry optimization, a conjugate Polak-Ribiere gradient was used with a termination gradient smaller than 10^{-3} kcal $Å^{-1}$ mol^{-1}. Molecular frontier orbitals (HOMO −9 to HOMO) were simulated directly on the force field-optimized structures using semiempirical extended Hückel theory.

Acknowledgements

Support by the Swiss National Science Foundation (grant 182082) is gratefully acknowledged. Financial support in France has been provided by the CNRS, the University of Angers and the Région Pays de la Loire through the RFI LUMOMAT (grant to K. M.). KHE thanks the Czech Science Foundation for financial support (grant No. 21-17194 L). Open Access funding provided by ETH-Bereich Forschungsanstalten.

Conflict of Interest

The authors declare no conflict of interest.

Data Availability Statement

The data that support the findings of this study are available from the corresponding author upon reasonable request.

Keywords: chirality · helicenes · on-surface chemistry · polyaromatic hydrocarbons · scanning tunneling microscopy

[1] a) V. Kohlschütter, *Z. Anorg. Allg. Chem.* **1919**, *105*, 1–25; b) M. D. Cohen, G. M. J. Schmidt, *J. Chem. Soc.* **1964**, *383*, 1996–2000.
[2] a) O. Stetsovych, M. Švec, J. Vacek, J. V. Chocholoušová, A. Jancarik, J. Rybáček, K. Kosmider, I. G. Stará, P. Jelínek, I. Starý, *Nat. Chem.* **2017**, *9*, 213–218; b) K.-H. Ernst, *Nat. Chem.* **2017**, *9*, 195–196; c) H. Chen, L. Tao, D. Wang, Z.-Y. Wu, J.-L. Zhang, S. Gao, W. Xiao, S. Du, K.-H. Ernst, H.-J. Gao, *Angew. Chem. Int. Ed.* **2020**, *59*, 17413–17416; *Angew. Chem.* **2020**, *132*, 17566–17569.
[3] a) L. Grill, S. Hecht, *Nat. Chem.* **2020**, 115–130; b) A. Sweetman, N. R. Champness, A. Saywell, *Chem. Soc. Rev.* **2020**, *49*, 4189–4202; c) T. Wang, J. Zhu, *Surf. Sci. Rep.* **2019**, *74*, 97–140; d) S. Clair, D. G. de Oteyza, *Chem. Rev.* **2019**, *119*, 4717–4776.
[4] a) Q. Shen, H.-Y. Gao, H. Fuchs, *Nano Today* **2017**, *13*, 77–96; b) C. Zhang, Z Yi, W. Xu, *Mater. Futur.* **2022**, *1*, 032301.
[5] a) F. Ullmann, J. Bielecki, *Ber. Dtsch. Chem. Ges.* **1901**, *34*, 2174–2185; b) M. Xi, B. E. Bent, *Surf. Sci.* **1992**, *278*, 19–32; c) M. Xi, B. E. Bent, *J. Am. Chem. Soc.* **1993**, *115*, 7426–7433; d) L. Grill, M. Dyer, L. Lafferentz, M. Persson, M. V. Peters, S. Hecht, *Nat. Nanotechnol.* **2007**, *2*, 687–691; e) M. Lackinger, *Chem. Commun.* **2017**, *53*, 7872–7885.
[6] a) Y. Shen, C.-F. Chen, *Chem. Rev.* **2012**, *112*, 1463–1535; b) T. Mori, *Chem. Rev.* **2021**, *121*, 2373–2412.
[7] M. Gingras, *Chem. Soc. Rev.* **2013**, *42*, 1051–1095.
[8] K.-H. Ernst, *Acc. Chem. Res.* **2016**, *49*, 1182–1190.
[9] Y. Yang, R. Correa da Costa, M. J. Fuchter, A. J. Campbell, *Nat. Photonics* **2013**, *7*, 634–638.
[10] K. Dhbaibi, L. Favereau, J. Crassous, *Chem. Rev.* **2019**, *119*, 8846–8953.
[11] F. Pop, N. Zigon, N. Avarvari, *Chem. Rev.* **2019**, *119*, 8435–8478.
[12] M. Kettner, V. V. Maslyuk, D. Nürenberg, J. Seibel, R. Gutierrez, G. Cuniberti, K.-H. Ernst, H. Zacharias, *J. Phys. Chem. Lett.* **2018**, *9*, 2025–2030.
[13] Y. Liang, K. Banjac, K. Martin, N. Zigon, S. Lee, N. Vanthuyne, F. A. Garcés-Pineda, J. R. Galán-Mascarós, X. Hu, N. Avarvari, M. Lingenfelder, *Nat. Commun.* **2022**, *13*, 3356.
[14] C. Wäckerlin, J. Li, A. Mairena, K. Martin, N. Avarvari, K.-H. Ernst, *Chem. Commun.* **2016**, *52*, 12694–12697.
[15] J. Li, K. Martin, N. Avarvari, C. Wäckerlin, K.-H. Ernst, *Chem. Commun.* **2018**, *54*, 7948–7951.
[16] A. Mairena, C. Wäckerlin, M. Wienke, K. Grenader, A. Terfort, K.-H. Ernst, *J. Am. Chem. Soc.* **2018**, *140*, 15186–15189.
[17] A. Mairena, M. Baljozović, M. Kawecki, K. Grenader, M. Wienke, K. Martin, L. Bernard, N. Avarvari, A. Terfort, K.-H. Ernst, C. Wäckerlin, *Chem. Sci.* **2019**, *10*, 2998–3004.
[18] C. Bronner, J. Björk, P. Tegeder, *J. Phys. Chem. C* **2015**, *119*, 486–493.
[19] L. Merz, K.-H. Ernst, *Surf. Sci.* **2010**, *604*, 1049–1054.
[20] A. Mairena, L. Zoppi, J. Seibel, A. F. Tröster, K. Grenader, M. Parschau, A. Terfort, K.-H. Ernst, *ACS Nano* **2017**, *11*, 865–871.
[21] R. Fasel, A. Cossy, K.-H. Ernst, F. Baumberger, T. Greber, J. Osterwalder, *J. Chem. Phys.* **2001**, *115*, 1020–1027.
[22] A. Mairena, M. Parschau, J. Seibel, M. Wienke, D. Rentsch, A. Terfort, K.-H. Ernst, *Chem. Commun.* **2018**, *54*, 8757–8760.
[23] B. Irziqat, A. Cebrat, M. Baljozović, K. Martin, M. Parschau, N. Avarvari, K. Ernst, *Chem. Eur. J.* **2021**, *27*, 13523–13526.
[24] S. Stolz, M. D. Giovannantonio, J. I. Urgel, Q. Sun, A. Kinikar, G. B. Barin, M. Bommert, R. Fasel, R. Widmer, *Angew. Chem. Int. Ed.* **2020**, *59*, 14106–14110; *Angew. Chem.* **2020**, *132*, 14210–14214.
[25] M. Fritton, D. A. Duncan, P. S. Deimel, A. Rastgoo-Lahrood, F. Allegretti, J. V. Barth, W. M. Heckl, J. Björk, M. Lackinger, *J. Am. Chem. Soc.c* **2019**, *141*, 4824–4832.
[26] a) R. H. Martin, M.-J. Marchant, *Tetrahedron Lett.* **1972**, *13*, 3707–3708; b) R. H. Martin, M. J. Marchant, *Tetrahedron* **1974**, *30*, 347–349.
[27] M. Jakubec, T. Beránek, P. Jakubík, J. Sýkora, J. Žádný, V. Církva, J. Storch, *J. Org. Chem.* **2018**, *83*, 3607–3616.

Manuscript received: January 15, 2023
Accepted manuscript online: March 1, 2023
Version of record online: March 28, 2023